



Editor invited article

Substantial curvature effects on compliant serpentine mechanics

Yafei Wang ^{a,1}, Wei Zhao ^{b,1}, Yangkun Du ^{c,1}, Zhijun Dai ^a, Yanju Liu ^{b,*}, Fan Xu ^{a,*}^a Institute of Mechanics and Computational Engineering, Department of Aeronautics and Astronautics, Fudan University, Shanghai, 200433, China^b Department of Astronautical Science and Mechanics, Harbin Institute of Technology, Harbin, 150001, China^c School of Mathematics and Statistics, University of Glasgow, Glasgow, G128QQ, UK

ARTICLE INFO

ABSTRACT

Keywords:

Large curvature
Curved beam
Flexibility and stretchability
Serpentine-based device
Optimization design

Serpentine interconnects (serpentines) with various degrees of curvature are often designed to absorb deformations and protect brittle active components in flexible devices. Serpentines with small curvature are modelled well using the traditional theory for doing so, but this overestimates the stretchability of serpentines with large curvature (e.g. the relative error exceeds 90%). Proposed here is a novel theoretical model in which a non-buckling serpentine is characterized as a large-curvature beam. Analytical solutions are derived, and systematic experiments and numerical simulations are reported to validate the accuracy and investigate geometrical dependence. It is found that (i) dimensionless geometrical parameters regulate the compliant mechanics of a serpentine, (ii) there is a certain arc angle that produces abnormal stretchability (i.e. the normalized stretchability is less than unity) and (iii) the flexibility and stretchability can be enhanced by between two and five orders of magnitude. This work offers a new way to construct optimal serpentine ribbons with large curvature for various applications.

1. Introduction

Modern advances in soft materials and manufacturing technology – particularly regarding extreme mechanics – have accelerated the development of flexible devices, which are the foundations for system-level biomedicine (Chung et al., 2020; Morikawa et al., 2019, 2018), optoelectronics (Ko et al., 2008; Yeo et al., 2013) and communication applications (Zhang et al., 2021; Fu et al., 2018; Jeong et al., 2013). These devices have significant advantages over well-established wafer-based technologies, such as having the flexibility and stretchability needed for sophisticated environments (Fan et al., 2014; Hong et al., 2015; Zhang et al., 2014); these properties are designed to withstand extreme deformation without losing electrical functionality. Specifically, high stretchability allows excessive elastic deformation and shields electrical components mechanically to avoid device failure, while high flexibility avoids having to impose mechanical restraints on the targeted biological tissues (Ma et al., 2016; Xu et al., 2013).

Flexible devices generally comprise active components and electrical interconnects (Chung et al., 2020; Morikawa et al., 2019, 2018; Ko et al., 2008; Yeo et al., 2013; Zhang et al., 2021; Fu et al., 2018; Jeong et al., 2013). Because the former are hard and brittle, they are attached to stiff islands that are permanently bonded to the flexible substrate (Guan et al., 2018b; Yang et al., 2018; Guan et al., 2018a).

and these are then networked by electronic interconnects to build a whole system for exchanging information with the outside environment. This effective design paradigm is known as the island–bridge architecture: the islands remain rigid, and the interconnects are largely responsible for absorbing any strain at system level (Someya et al., 2004; Brosteaux et al., 2007; Kim et al., 2008; Yeo et al., 2013; Jeong et al., 2013). However, to maintain excellent device performance, the stiff islands must cover a large area, leaving less design space for electrical interconnects. Therefore, the main challenge with these electrical interconnects is how to integrate responses with extremely high flexibility and stretchability within limited space. To date, many design strategies for electrical interconnects have been developed, including geometry-dependent serpentine design (Someya et al., 2004; Brosteaux et al., 2007), fractal patterns (Fan et al., 2014) and origami/kirigami motifs (Kim et al., 2008; Yeo et al., 2013; Jeong et al., 2013; Xu et al., 2013). As evident from Fig. 1, of all these paradigms, the mechanics and geometry design for serpentine ribbons are particularly prominent (Someya et al., 2004; Brosteaux et al., 2007; Kim et al., 2008; Yeo et al., 2013; Jeong et al., 2013; Xu et al., 2013; Fan et al., 2014; Zhang et al., 2014; Jang et al., 2015; Xu et al., 2015; Liu et al., 2016a; Jang et al., 2017; Fu et al., 2018; Kim et al., 2021; Hwang et al., 2022), with curvature playing a significant role in creating the extreme mechanics of geometry-dependent serpentines.

Invited Editor: Yihui Zhang.

* Corresponding authors.

E-mail addresses: yj_liu@hit.edu.cn (Y. Liu), fanxu@fudan.edu.cn (F. Xu).¹ These authors contributed equally to this work.

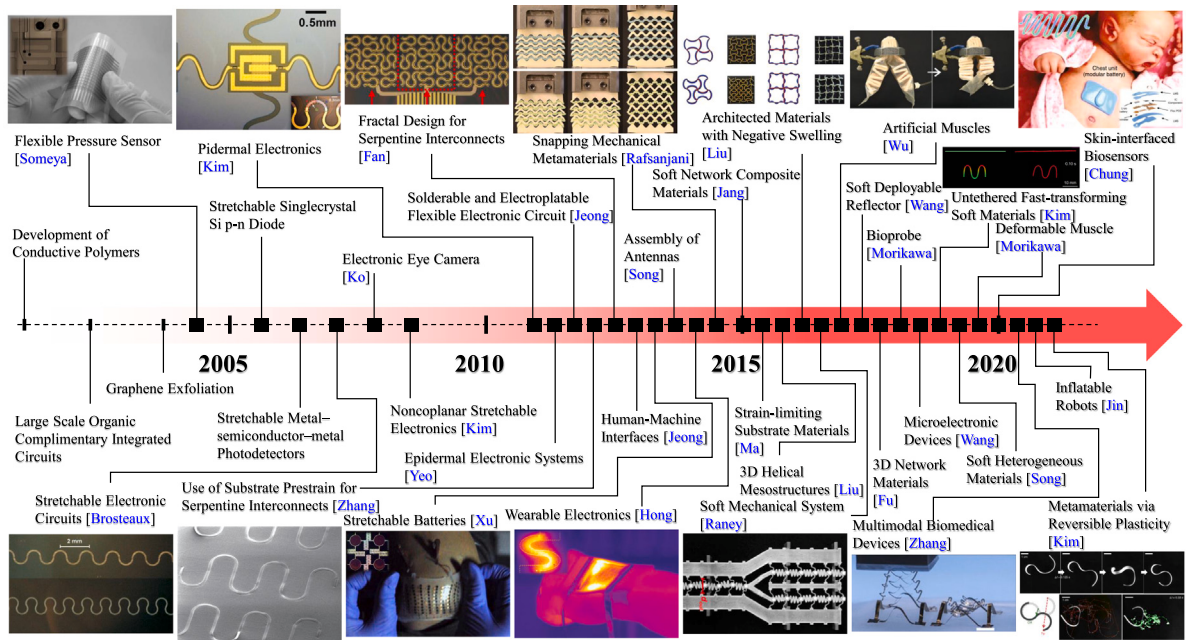


Fig. 1. Recent advancements in mechanics, materials and applications for the ultrastretchable serpentine-based flexible devices. (Online version in colour.)

Recently, two different serpentine classifications have been advanced for investigating serpentine-engineered elasticity (Zhang et al., 2014; Fan et al., 2016; Widlund et al., 2014; Yang et al., 2017; Pan et al., 2017), these being based on the ratio \bar{w} of beam width to curvature radius. The first type of serpentine ribbon (i.e. those with $\bar{w} < 0.2$) provides lower electrical resistance for functional devices such as radiofrequency coils (Brosteaux et al., 2007), while the second type involves a curved beam with $\bar{w} \geq 0.2$ —known as a large-curvature beam (LCB)—and is widespread in flexible devices and offers a wider range of applications (Fu et al., 2018; Kim et al., 2021; Hwang et al., 2022; Zhang et al., 2014; Fan et al., 2016; Widlund et al., 2014; Yang et al., 2017; Pan et al., 2017). Timoshenko & Goodier (Timoshenko, 1951) compared elasticity theory with LCB theory and classical beam theory for the pure bending of curved beams, discovering that the elasticity and LCB solutions agreed well; for $\bar{w} < 0.2$, the relative error of the pure-bending normal stress between beam theory and the LCB solution was always less than 7%, but using beam theory to assess LCBs was inappropriate because of their significant margin of relative error for $\bar{w} > 0.2$. Therefore, to appreciate the fundamental relationship among flexibility, stretchability, and geometry, a theoretical model for serpentine ribbons with various degrees of curvature (Zhang et al., 2014; Fan et al., 2016; Widlund et al., 2014; Yang et al., 2017; Pan et al., 2017) must be developed. To the best of our knowledge, the implications of significant curvature on the compliant mechanics of serpentines are yet to be studied, and the issue of stretchability-related abnormal mechanics has received relatively little attention. The only related work involved creating a theoretical model of beams without accounting for large curvature (Fan et al., 2016; Widlund et al., 2014; Pan et al., 2017; Cicconofri and DeSimone, 2015; Yin et al., 2019), thereby failing to foresee the need for large-curvature serpentine ribbons in flexible devices. Even though a complex elasticity theory (Yang et al., 2017) based on approximating boundary conditions has been developed for serpentines with particular geometries, it is not easily applicable to the optimization design and analyses of serpentine ribbons, as required for maximum stretchability under geometrically constrained conditions or limited spaces (Hwang et al., 2022; Jin et al., 2021; Zhang et al., 2021; Kim et al., 2018; Li et al., 2017; Raney et al., 2016; Liu et al., 2016b; Rafsanjani et al., 2015).

In the present study, a theoretical model for an ultrastretchable non-buckling serpentine ribbon as an LCB (e.g. $\bar{w} = 1$) is developed and confirmed using experiments, numerical computations and precise elasticity theory. The overall concept that emerges offers a paradigm for designing serpentine ribbons that are as flexible and stretchable as possible. The paper is structured as follows. The analytical strategy from the energy principle is summarized in Section 2. In Section 3, several theoretical solutions are compared, and it is shown how flexibility and stretchability rely on geometry. The experimental validation is also presented in Section 3 together with the numerical and experimental methodologies. The optimal design technique is illustrated in Section 4, and a summary is provided in Section 5.

2. Theoretical model

Here, we design the serpentine ribbon as a unidirectional periodic material; see Fig. 2a for details and Fig. 2b for its typical unit cell. In the analytical model, the radius R and arc angle α describe the arc sections, the arm section of length l is the unique geometrical element for expanding the design space, and the maximum distances for the unit cell in the x and y directions are L_x and L_y , respectively, as shown in Fig. 2b. The end-to-end length of the unit cell is determined by

$$L_x = 4(R \cos \alpha - l \sin \alpha), \quad (1)$$

and if the arc angle is specified as $\alpha = -\pi/2$, then the serpentine ribbon becomes a straight beam of length $L_x = 4l$.

These fundamental assumptions allow us to build a dimensionless closed-form theory that involves three independent dimensionless geometrical parameters, i.e. $\bar{w} = w/R$, α and $\bar{l} = l/R$; note that different combinations of these three parameters can be used to investigate different serpentine designs. Here, we develop the expanded formulas for a serpentine ribbon as an LCB based on the energy method.

The purpose of the present study is to develop a method for designing the flexibility and stretchability of a family of serpentine ribbons using an LCB ($\bar{w} \geq 0.2$). Fig. 2c shows how the simplified analytical model is carefully built for any geometrical alterations for this purpose. The left end of the LCB is assumed to be a hinged support, and the simplified model is loaded with a force F and a moment M_o assuming that its right end is free. The closed-form solutions for the normalized

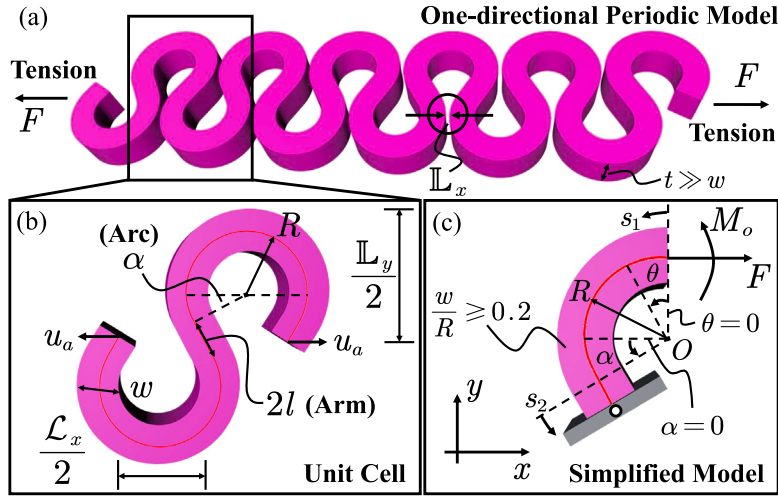


Fig. 2. Illustrations of the serpentine unit cell and simplified model with prescribed geometry parameters and boundary conditions labelled. (a) One-directional Periodic Model of the serpentine ribbon. (b) The representative unit cell with associated geometric parameters. (c) The simplified model and its boundary conditions. (Online version in colour.)

flexibility and stretchability are determined using the energy method from plane-strain beam theory and LCB theory; see [Appendix A](#) for details. In particular, the normalized flexibility D (corresponding to a straight beam of length L_x) is given by

$$D = 2u_a EA/FL_x, \quad (2)$$

where u_a is the applied displacement corresponding to F (for details, see Eq. [\(A.1\)](#) in [Appendix A](#)), and E and A are the plane-strain modulus and the cross-sectional area, respectively. The second key index is the normalized stretchability \mathcal{E} , which is calculated as

$$\mathcal{E} = \epsilon_a^f / \epsilon_m^f = \epsilon_a / \epsilon_{\max}, \quad (3)$$

where ϵ_a^f and ϵ_m^f are the elastic stretchability (i.e., the maximum strain that can be achieved in the elastic deformation range of the serpentine ribbon under tension) and intrinsic failure strain, respectively. Corresponding to u_a , here ϵ_a is the applied strain, and ϵ_{\max} is the maximum strain of the LCB. It is important to note that the failure criterion ([Wang and Wang, 2021, 2020, 2022; Wang et al., 2020](#)) is determined using

$$\epsilon_m^f = \epsilon_{\max}, \quad (4)$$

and for premium inorganic electronic materials such as silicon and nitride dielectrics, the related rupture strain is represented by ϵ_m^f .

The following relationships allow the energy approach to be used to determine the normalized flexibility and stretchability in terms of the dimensionless geometrical parameters \bar{w} , α and \bar{l} :

$$\begin{aligned} D &= D(\bar{w}, \alpha, \bar{l}, J(\bar{w})) = (\bar{w}^4 d_1 + J^2 d_2 + J \bar{w}^2 d_3 + \cos(2\alpha) d_4 \\ &\quad + \sin(2\alpha) d_5) / d_6, \\ \mathcal{E} &= \mathcal{E}(\bar{w}, \alpha, \bar{l}, J(\bar{w})) = (\bar{w}^4 d_1 + J^2 d_2 + J \bar{w}^2 d_3 + \cos(2\alpha) d_4 \\ &\quad + \sin(2\alpha) d_5) / d_7, \end{aligned} \quad (5)$$

where $J = 1 - \bar{w}/(\ln(2 + \bar{w}) - \ln(2 - \bar{w}))$ is associated with the large-curvature effect. The explicit forms ($d_1 \sim d_7$) of D and \mathcal{E} are given in [Appendix A](#); see Eqs. [\(A.10\)](#) and [\(A.15\)](#).

Curvilinear coordinates and elasticity theory (the Airy stress function) are used to find the precise solutions for various geometries to understand fully how large curvature affects D and \mathcal{E} for ultra-stretchable serpentine ribbons; see [Appendix B](#) for further information. Also, by either taking the expansion of $\ln(b/a)$ in elasticity theory [for details, see Eq. [\(C.1\)](#) to three orders] or neglecting the curvature effects in LCB theory [for details, see Eq. [\(C.3\)](#) and $y/R(1 - J) \ll 1$ in [Appendix C](#)], the degenerate analytical LCB solutions [i.e. the solutions of so-called conventional beam (CB) theory] are demonstrated in [Appendix C](#). In [Appendix D](#), particular analytical solutions are refined to

give important results for constructing flexible devices experimentally; for example, in the case of $\alpha = \bar{l} = 0$, we have the following brief expressions:

$$\begin{aligned} D &\approx 103\pi/100 + 3(\pi^2 - 8)/\pi\bar{w}^2, \\ \mathcal{E} &\approx (\pi^2(300 + 103\bar{w}^2) - 2400)/600(\pi - 2)\bar{w}. \end{aligned} \quad (6)$$

However, because of the intricacy of the general closed-form solutions, more research is required to determine how geometry, material, and significant curvature affect the normalized flexibility and stretchability, and the next sections detail this procedure. Additionally, it is critical to recognize that for non-buckling serpentine structures, the generalized theoretical model elaborated in this paper offers substantial insight into the correlation between flexibility, stretchability, and various dimensionless geometric parameters. However, the assumption disregarding nonlinear deformation effects is not applicable to serpentine structures that endure substantial deformation prior to structural failure. Predictions grounded in infinitesimal deformation theory might lead to considerable overestimation of stretchability when compared to those based on finite deformation theory. Future investigations will focus on the interplay of significant curvature and finite deformation effects in serpentine structures.

3. Results and discussion

3.1. Experimental demonstration

Using a high-precision universal testing system (model 5965; Instron, USA), tensile experiments were carried out to subject serpentine ribbons to quasistatic loading. The samples were designed using solid modelling software and then 3D printed in resin (UV curing). To avoid lateral buckling, we selected a large thickness-to-width ratio (such as $t/w > 10$). For a nonbuckling serpentine ribbon, the specimen was clamped carefully with skidproof chunks on the tensile tester, and then using a high-resolution camera, the geometrical deformation of the serpentine ribbon was captured as precisely as possible. Based on the accurate stress-strain curves generated from the tests, we can determine the flexibility, elastic stretchability and intrinsic failure strain for a straight beam and a serpentine ribbon with the same end-to-end length. Finally, according to Eq. [\(5\)](#), experimental verification is possible for the corresponding mechanical parameters. Our findings using the LCB model should be relevant and applicable for engineering scenarios over a wide variety of length scales once the practical results are found to agree with the theoretical solutions and numerical simulations.

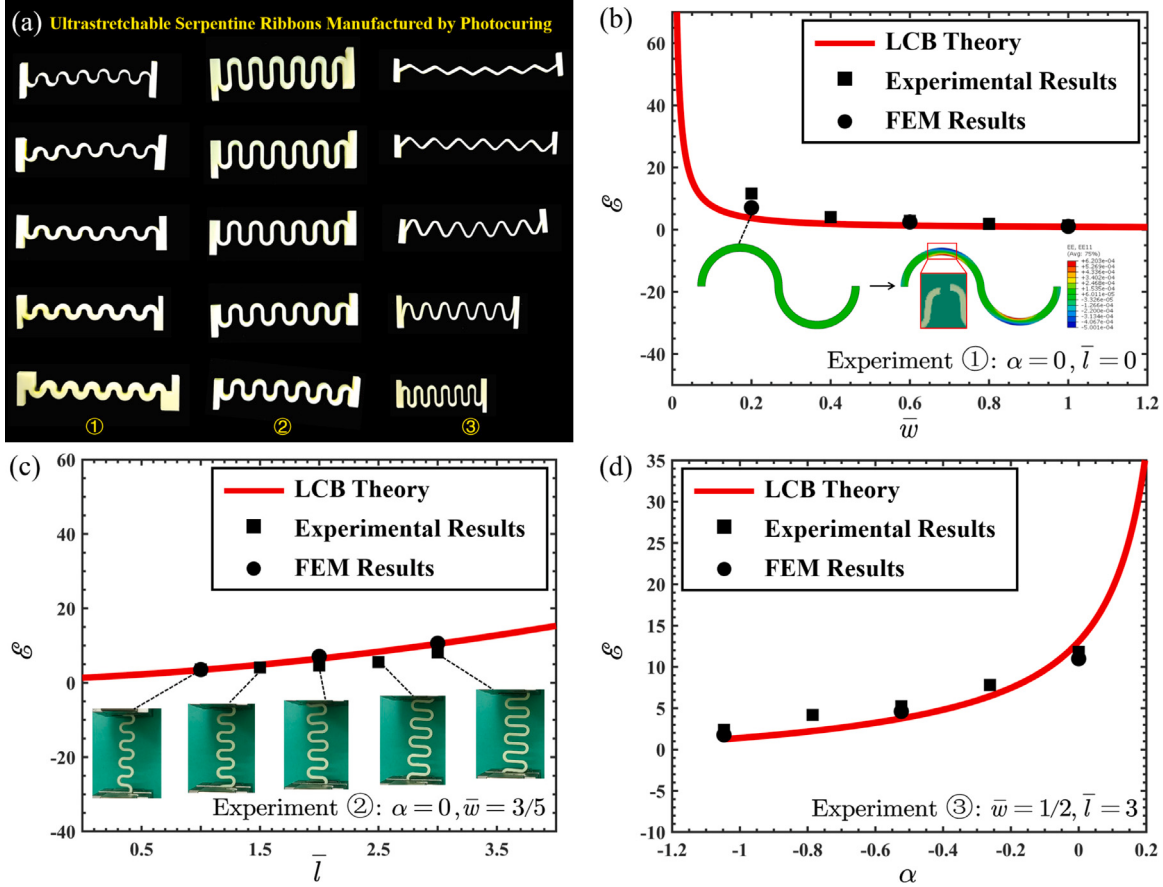


Fig. 3. Experimental samples and comparison of the theoretical, numerical and experimental results for the normalized stretchability of the serpentine ribbon. (a) 3D-printing samples (UV curing technique). (b) Comparison of experimental data, LCB solutions and FEM results for the normalized stretchability when $\alpha = \bar{l} = 0$. (c) Comparison of experiments, LCB solutions and FEM results for the normalized stretchability when $\alpha = 0$ and $\bar{w} = 3/5$. (d) Comparison of experiments, LCB solutions and FEM results for the normalized stretchability when $\bar{w} = 1/2$ and $\bar{l} = 3$. (Online version in colour.)

Numerical analysis was performed using ABAQUS software, with the plane-strain finite-element method (FEM) and Eq. (3) used to simplify the problem. For high-quality inorganic silicon, its Young's modulus and Poisson ratio are 130 GPa and 0.27, respectively, and according to the basic assumptions of elasticity theory, the applied strain can be taken as 0.01. Finally, to ensure accuracy, all the simulations involved refined meshes.

Fig. 3 compares the normalized stretchability as given by our theory, experiments and FEM results. Moreover, the force-displacement curves obtained from the experiments are provided in Appendix E. The prevention of lateral buckling for the 3D printed samples in Fig. 3a ensured that the serpentine ribbons deformed entirely in-plane. Without the arc angle and arm section, Fig. 3b shows the stretchability as a function of ribbon width. Similar to the theoretical predictions, the serpentine ribbon generally breaks on the inside of the curved beam (see the FEM and experimental results in Fig. 3b). The evolution of stretchability in relation to arm length is seen in Fig. 3c. With a constant ribbon width and arm length, Fig. 3d shows the stretchability as a function of arc angle. The experimentally determined normalized stretchability is in strikingly good agreement with the analytical solution, as shown in Fig. 3. By combining LCB theory, the dimensionless model and the energy principle, the findings are quite precise. These results imply that our findings can be extended to large-curvature serpentine ribbons while maintaining ultra-high stretchability, going beyond the narrow serpentines as used originally.

3.2. Comparison of theories

The main mechanical characteristics of serpentine ribbons are revealed using plane-strain elasticity theory, LCB theory and CB theory.

In elasticity theory, we can calculate the displacement field caused by the specified loading. Finally, according to Eq. (3), the normalized stretchability $\mathcal{E}_{\text{Elasticity}}$ based on elasticity theory can be calculated using the following elegant form:

$$\mathcal{E}_{\text{Elasticity}} = a(b^2 + a^2)\pi/(b-a)(b+a)^2, \quad (7)$$

where $a = R - w/2$ and $b = R + w/2$. The detailed form of Eq. (7) is given in Appendix B: see Eq. (B.19).

The conventional theory can then be formed using the series expansion approach. By taking the expansion of $\ln(b/a) = ua^{-1} - w^2/2a^2 + w^3/3a^3$ to three orders and neglecting the higher-order terms [see Eqs. (C.1) and (C.2) in Appendix C for details], the displacement field can be refined. Equally, based on Eq. (3), the normalized stretchability \mathcal{E}_{CB} from CB theory can be given as

$$\mathcal{E}_{\text{CB}} = (\tilde{d}_1 + \cos(2\alpha)\tilde{d}_2 + \sin(2\alpha)\tilde{d}_3)/\tilde{d}_5, \quad (8)$$

where $\tilde{d}_1, \tilde{d}_2, \tilde{d}_3$ and \tilde{d}_5 are functions of the dimensionless geometrical parameters. The explicit form of Eq. (8) is given in Appendix C: see Eqs. (C.11) and (C.12) for details.

For a good grasp of how significant curvature influences stretchability, the relative error δ [%] between LCB theory and CB theory is defined as

$$\delta = (|\mathcal{E}| - |\mathcal{E}_{\text{CB}}|)/|\mathcal{E}| \times 100\%, \quad (9)$$

where \mathcal{E} is the normalized stretchability from LCB theory as given by Eq. (5).

Fig. 4 compares elasticity theory, LCB theory and CB theory according to Eqs. (5), (7) and (8). With increasing \bar{w} (resp. \bar{l}), \mathcal{E} decreases

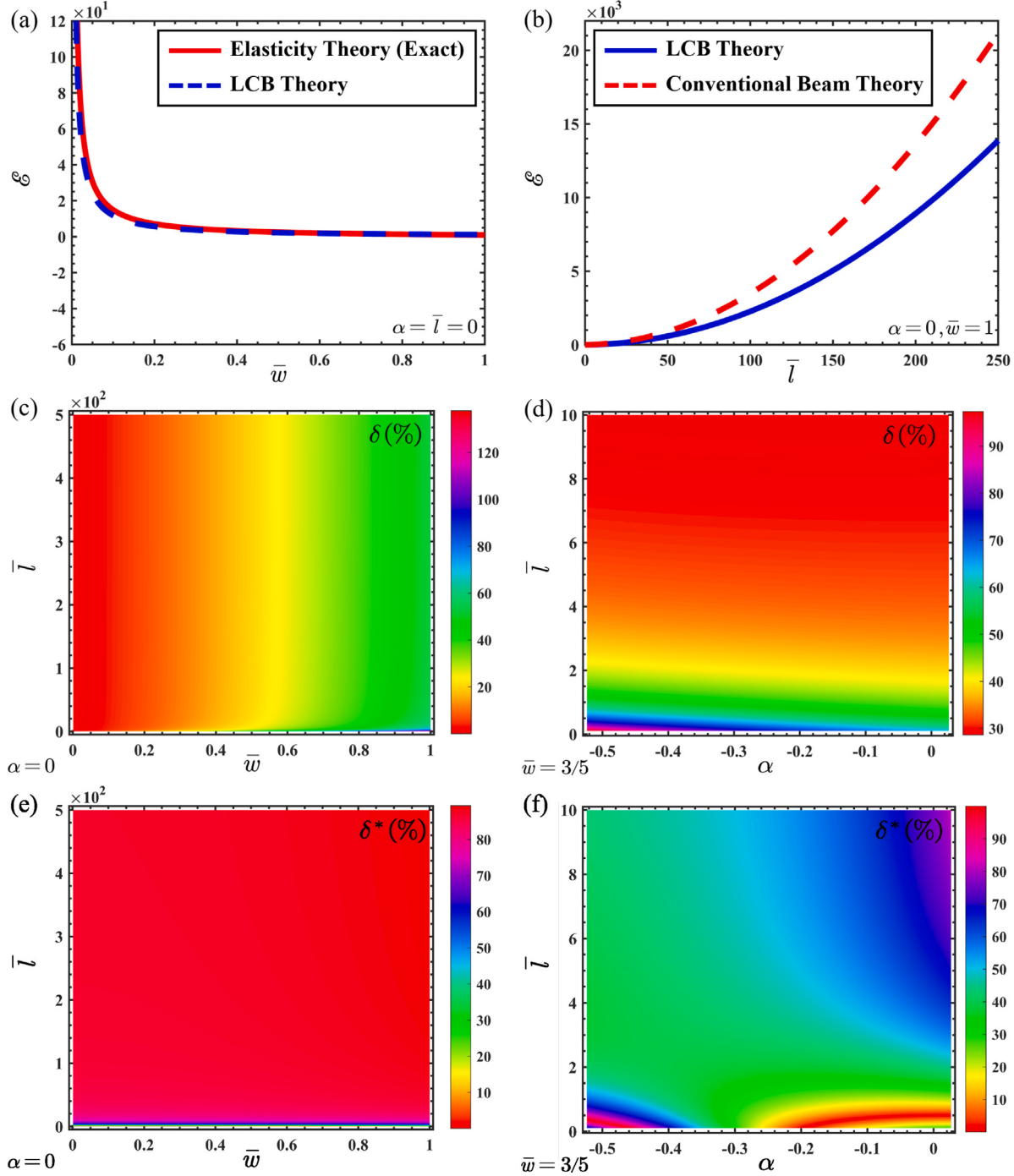


Fig. 4. Comparison of the elasticity theory, LCB theory and conventional beam (CB) theory, and distribution of the relative error with respect to the normalized stretchability. (a) Comparison of theoretical results for normalized stretchability as the function of \bar{w} based on the exact elasticity theory and our LCB theory. (b) Comparison of theoretical results for normalized stretchability as the function of \bar{l} based on our LCB theory and CB theory. (c) Distribution of the relative error between the LCB theory and CB theory when $\alpha = 0$. (d) Distribution of the relative error between the LCB theory and CB theory when $\bar{w} = 3/5$. (e) Distribution of the relative error between the LCB theory and Widlund's curved beam theory (Widlund et al., 2014) when $\alpha = 0$. (f) Distribution of the relative error between the LCB theory and Widlund's curved beam theory (Widlund et al., 2014) when $\bar{w} = 3/5$. (Online version in colour.)

(resp. increases). The closed-form LCB solution agrees quite well with the solution from elasticity theory for the particular shape in Fig. 4a. This implies that both theories can predict ε accurately over a wide range of \bar{w} (such as $\bar{w} \geq 0.2$). However, LCB theory and CB theory differ significantly in Fig. 4b, which indicates that simple bending strain is insufficient for defining large-curvature serpentine ribbons.

For $\bar{w} < 0.2$, LCB theory and CB theory are related [see Eqs. (C.3) and (C.4) in Appendix C for details], this being because the crucial integral $\int_A y^2/(1+y/R(1-\mathcal{J}))dA$ degenerates into what is known as

the second-area moment. When y and $R(1-\mathcal{J})$ are comparable rather than $y \ll R(1-\mathcal{J})$ (i.e. very slender serpentine), it is difficult to obtain precise results for normalized stretchability by using CB theory. For example, in Fig. 4c the relative error δ is as high as 120%, and in Fig. 4d it reaches 90%.

In addition, we compare the LCB theory with the Widlund's curved beam theory (Widlund et al., 2014). The large curvature effect of the serpentine is neglected in their theory. Using the same geometric parameters, we can also define the relative error δ^* between the LCB

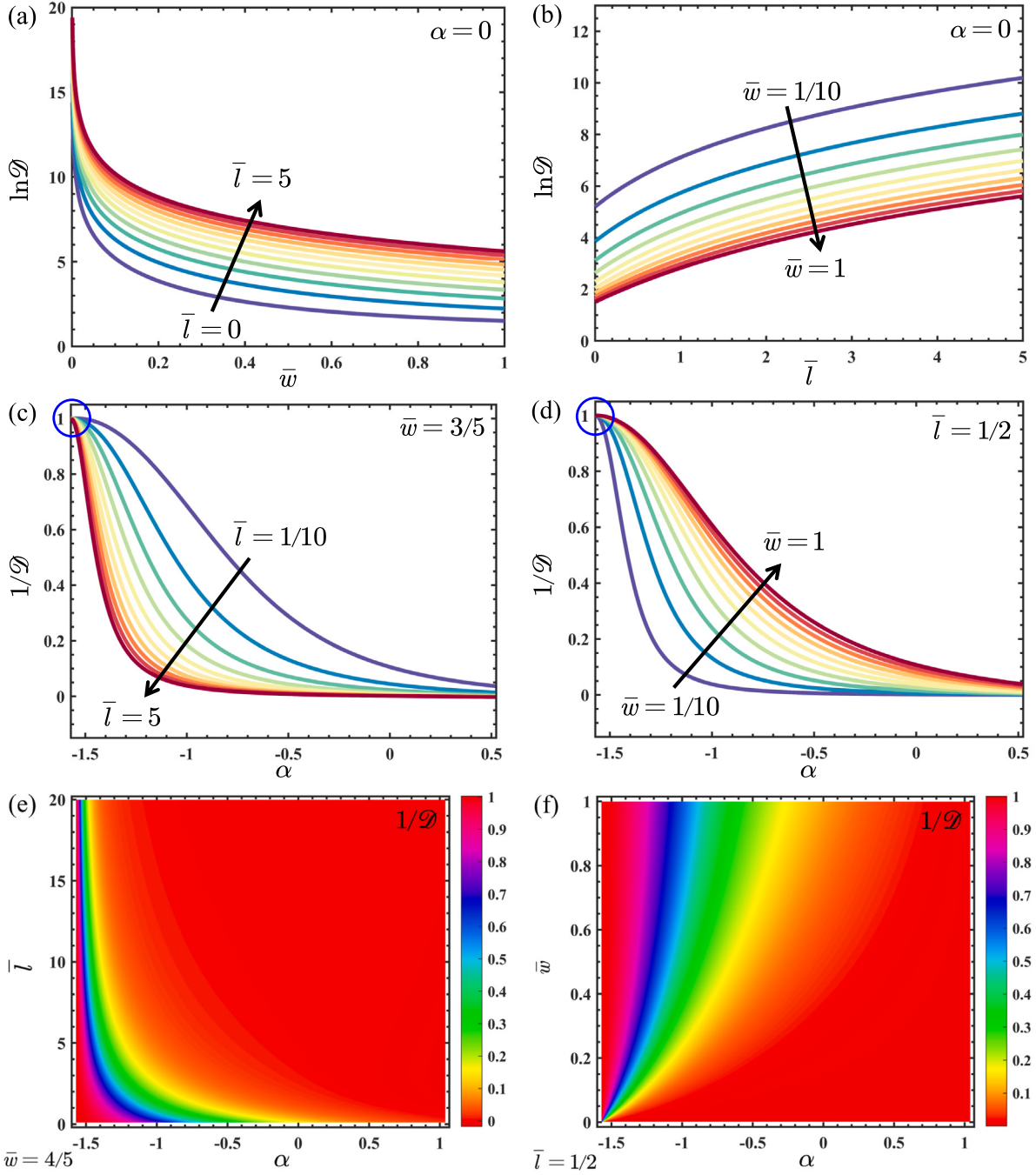


Fig. 5. Geometry dependence and distribution of the normalized flexibility \mathcal{D} for the different dimensionless geometry parameters \bar{w} , α and \bar{l} . (a) The natural logarithm of normalized flexibility versus \bar{w} when $\alpha = 0$ and $0 \leq \bar{l} \leq 5$. (b) The natural logarithm of normalized flexibility versus \bar{l} when $\alpha = 0$ and $1/10 \leq \bar{w} \leq 1$. (c) The reciprocal of normalized flexibility as the function of α when $\bar{w} = 3/5$ and $1/10 \leq \bar{l} \leq 5$. (d) The reciprocal of normalized flexibility as the function of α when $\bar{l} = 1/2$ and $1/10 \leq \bar{w} \leq 1$. (e) Distribution of the reciprocal of normalized flexibility when $\bar{w} = 4/5$. (f) Distribution of the reciprocal of normalized flexibility when $\bar{l} = 1/2$. (Online version in colour.)

theory and the Widlund's curved beam theory. Equally, curved beam theory gives imprecise results for the serpentine with large curvature. Corresponding to the geometric parameters in Fig. 4c and d, the relative errors δ^* are as high as 80% (see Fig. 4e) and 90% (see Fig. 4f), respectively.

In summary, large curvature appears to play a significant role in the underlying mechanics of serpentine ribbons, and we recommend that the analytical modelling and accompanying device design be carried out with caution. Geometrical sensitivity and dependence regarding various mechanical aspects are still unresolved issues that merit additional investigation.

3.3. Geometrical dependence of flexibility

Based on LCB theory, Fig. 5 shows the geometry dependency of the normalized flexibility with reference to the serpentine ribbon (see Appendix A for details). The impacts of the ribbon width-to-radius ratio \bar{w} and the arm length-to-radius ratio \bar{l} on the natural logarithm of the normalized flexibility are shown specifically in Fig. 5a and b. Naturally, the normalized flexibility decreases with increasing \bar{w} for fixed \bar{l} , and a longer arm length results in considerably increased normalized flexibility \mathcal{D} for given \bar{w} . Fig. 5c and d show how the arc angle α influences the reciprocal $1/\mathcal{D}$ of the normalized flexibility

for varying \bar{w} and \bar{l} . The flexibility D increases with increasing α , and increasing \bar{w} results in a lower D for given α . Nevertheless, three essential characteristics should be mentioned. (1) For $\alpha = -\pi/2$, the serpentine ribbon becomes a straight beam, from which follows that the normalized flexibility D is unity according to Eqs. (5) and (A.1) (or $1/D = 1$; see Fig. 5c and d for details). (2) Because the arc angle is limited mathematically by the non-overlapping nature of serpentine ribbons as LCBs, further research on ultrastretchable serpentines should also incorporate optimization design and analysis. (3) While the geometry dependences of \bar{w} , α and \bar{l} regarding D are all monotonic, increasing the arm length can in fact improve the normalized flexibility significantly (such as $D = e^{10.2} = 26903.2$ (i.e., the flexibility can be enhanced by 5 orders of magnitude) in the case of $\alpha = 0$, $\bar{l} = 5$ and $\bar{w} = 0.1$). These events – which result from the same long-arm effects as in Fig. 5b – offer significant proof of ultra-high flexibility for biomedical devices for health monitoring (Yeo et al., 2013; Song et al., 2020; Sim et al., 2020; Hong et al., 2019; Ashley et al., 2019) and precision therapy (Hong et al., 2015, 2019; Wu et al., 2017; Song et al., 2019), energy devices (Hwang et al., 2022; Zhang et al., 2021; Rafsanjani et al., 2015) and antennas (Wang et al., 2017; Song et al., 2014; Zhu et al., 2019), as well as artificial metamaterials (Liu et al., 2016b; Zhang et al., 2021; Coulais et al., 2016; Frenzel et al., 2016; Shan et al., 2015) (such as unusual swelling behaviour, thermal expansion, multistability and programmability).

Fig. 5e and f show the distributions of the normalized flexibility for independent \bar{w} , α and \bar{l} . The phase distribution diagrams offer an additional theoretical tool for developing extreme mechanics, where serpentine-shaped patterns are used to create new classes of ultra-high-flexibility mechanisms that take advantage of the geometry dependency. Also, the contour diagrams provide in-depth knowledge about the graphs in Fig. 5a–d.

3.4. Geometrical dependence of stretchability

Fig. 6 shows how geometry affects the normalized stretchability \mathcal{E} of the serpentine ribbon as an LCB. From Fig. 6a and b, we conclude that both evolutions of $1/\mathcal{E}$ are monotonic. The reciprocal of the normalized stretchability increases with increasing \bar{w} , suggesting that in principle a wider ribbon always suppresses its in-plane rotation. The corresponding tendency is inverted as the arm length is increased; specifically, a serpentine ribbon with larger \bar{w} and smaller \bar{l} can experience far more bending strain than can a thin one. With increasing arc angle α , Fig. 6c and d show more information about the geometry dependence of the normalized stretchability. First, a monotonic increase of $1/\mathcal{E}$ followed by a drop from its maximum value, after which it varies in a narrow range. However, the following three results are notable. (1) For $\alpha = -\pi/2$, the serpentine ribbon becomes a straight beam, therefore we have $1/\mathcal{E} = \mathcal{E} = 1$. (2) The theoretical solutions show that in some cases, $1/\mathcal{E} = \varepsilon_{\max}/\varepsilon_a$ [see equation (3) for details] can exceed unity, which indicates that the peak strain ε_{\max} may exceed the applied strain ε_a . (3) The normalized stretchability of the serpentine ribbon can still be increased significantly by long-arm effects (such as $\mathcal{E} = 17.6056$ (that is, the stretchability can be enhanced by 2 orders of magnitude) for $\alpha = 0.1$, $\bar{l} = 0.5$ and $\bar{w} = 0.1$), and the corresponding contributions and ensuing extremely high stretchability are consistent with earlier experiments, such as those for epidermal electronics (Jeong et al., 2013; Kim et al., 2011; Yeo et al., 2013), fingertip electrotactile actuators (Li et al., 2017; Jeong et al., 2013; Jang et al., 2015, 2017), ultrastretchable batteries (Xu et al., 2013) and high-performance flexible electronics (Yin et al., 2019; Jeong et al., 2012; Someya et al., 2004; Hong et al., 2019; Song et al., 2020; Wang and Wang, 2022). These findings show clearly that careful normalized-stretchability design based on the appropriate theories is necessary, because not all serpentine geometries give increased \mathcal{E} . For instance, if we choose an improper shape, then the peak strain will be larger than the applied strain, resulting in $1/\mathcal{E} > 1$ and $\mathcal{E} < 1$. In

Section 4, we report a study of the optimal design of \mathcal{E} with a number of geometrically limited requirements to circumvent this problem.

Finally, Fig. 6e and f show the phase distribution diagrams of $1/\mathcal{E}$ for $-\pi/2 \leq \alpha \leq \pi/6$, $0 \leq \bar{w} \leq 1$ and $0 \leq \bar{l} \leq 50$. The potential for increasing the stretchability of serpentine ribbons greatly by several orders of magnitude is realized by having broader dimensionless geometries.

4. Optimization design

It is crucial and necessary to understand better the stretchability of serpentine ribbons under the geometrical constraints imposed by non-overlapping geometry and existing technological bottlenecks (such as the restricted resolution of photolithography Widlund et al., 2014; Wang et al., 2020). In this case, we report a serpentine optimization study to obtain the greatest stretchability based on LCB theory. Obviously, from Figs. 2 and 7a, the length \mathbb{L}_x controls the minimum distance between two adjacent unit cells, which signifies that \mathbb{L}_x is non-negative (i.e. $\mathbb{L}_x = \mathbb{L}_x/R \geq 0$). Simultaneously, from the geometrical analysis (see Fig. 7a for details), we have the following equations to calculate the nonnegative \mathbb{L}_x and dimensionless length $\bar{\mathbb{L}}_x$:

$$\mathbb{L}_x = 2(\mathbb{L}_x^a - \mathbb{L}_x^b - \mathbb{L}_x^c) \geq 0 \Rightarrow \bar{\mathbb{L}}_x = 2(\bar{\mathbb{L}}_x^a - \bar{\mathbb{L}}_x^b - \bar{\mathbb{L}}_x^c) \geq 0, \quad (10)$$

where $\bar{\mathbb{L}}_x^a = (1 - \bar{w}/2) \cos \alpha$, $\bar{\mathbb{L}}_x^b = 2\bar{l} \sin \alpha$ and $\bar{\mathbb{L}}_x^c = (1 + \bar{w}/2)(1 - \cos \alpha)$.

The next step is to identify the second condition, i.e. the geometrical constraint. As evident from Figs. 2 and 7a, we can first designate a minimum in-plane length $\bar{\mathbb{L}}_y = \mathbb{L}_y/R = \xi \bar{w}$ to generate the serpentine ribbon with maximum stretchability, where ξ is a prefactor and reflects the degree of geometrical restriction. According to Fig. 7a, the dimensionless in-plane length $\bar{\mathbb{L}}_y$ is calculated as

$$\bar{\mathbb{L}}_y = \xi \bar{w} = 2(1 + \bar{w}/2 + \sin \alpha + \bar{l} \cos \alpha). \quad (11)$$

With these fundamental assumptions, combining Eqs. (5), (10) and (11) gives Fig. 7b to achieve the maximum stretchability (\mathcal{E}_{\max} or $(1/\mathcal{E})_{\min}$) for the serpentine ribbon. The degree of geometrical restriction ranges from $\xi = 6$ to 26, and the black dots in Fig. 7b correspond to the optimal geometries based on LCB theory. It is important to note that the colour bar in Fig. 7b represents the reciprocal of the normalized stretchability. With the optimal parameters $(\bar{w})_{Optimization}$ and $(\bar{l})_{Optimization}$, the maximum arc angle $(\alpha)_{\max}$ can be identified according to the non-negativity of Eq. (10). Fig. 7c shows the optimal designs and results for various ξ (i.e. $6 \leq \xi \leq 26$). As a demonstration, if we designate the in-plane breadth of the serpentine ribbon as being six times larger than \bar{w} , then the optimal shape with maximum stretchability is given by $\{\bar{l}, \bar{w}, \alpha\} = \{0.122, 0.699, 0.715\}$. The accuracy of our optimization technique is comparable to that of the Lagrangian-multiplier optimization approach, and finally note that it is a straightforward, quick and efficient way of determining the maximum stretchability.

5. Conclusion

The results presented herein show the significant curvature effects of ultrastretchable serpentine ribbons for flexible devices using LCB theory, elasticity theory, CB theory, FEM calculations and experiments. The precise LCB and elasticity solutions shed light on the geometrical dependences of normalized flexibility and stretchability. Our research shows that serpentine ribbons with long arms and narrow ribbons are extremely flexible and stretchable; via the long-arm effects, the flexibility and stretchability can be increased by between two and five orders of magnitude. The relative error between LCB and CB solutions is more than 90%, and the arc angle has a significant impact on abnormal stretchability (i.e. the normalized stretchability is less than one). Along with an optimization design with geometrical restrictions, these results suggest that a large distribution of dimensionless parameters and a related database would be helpful for expediting the search for

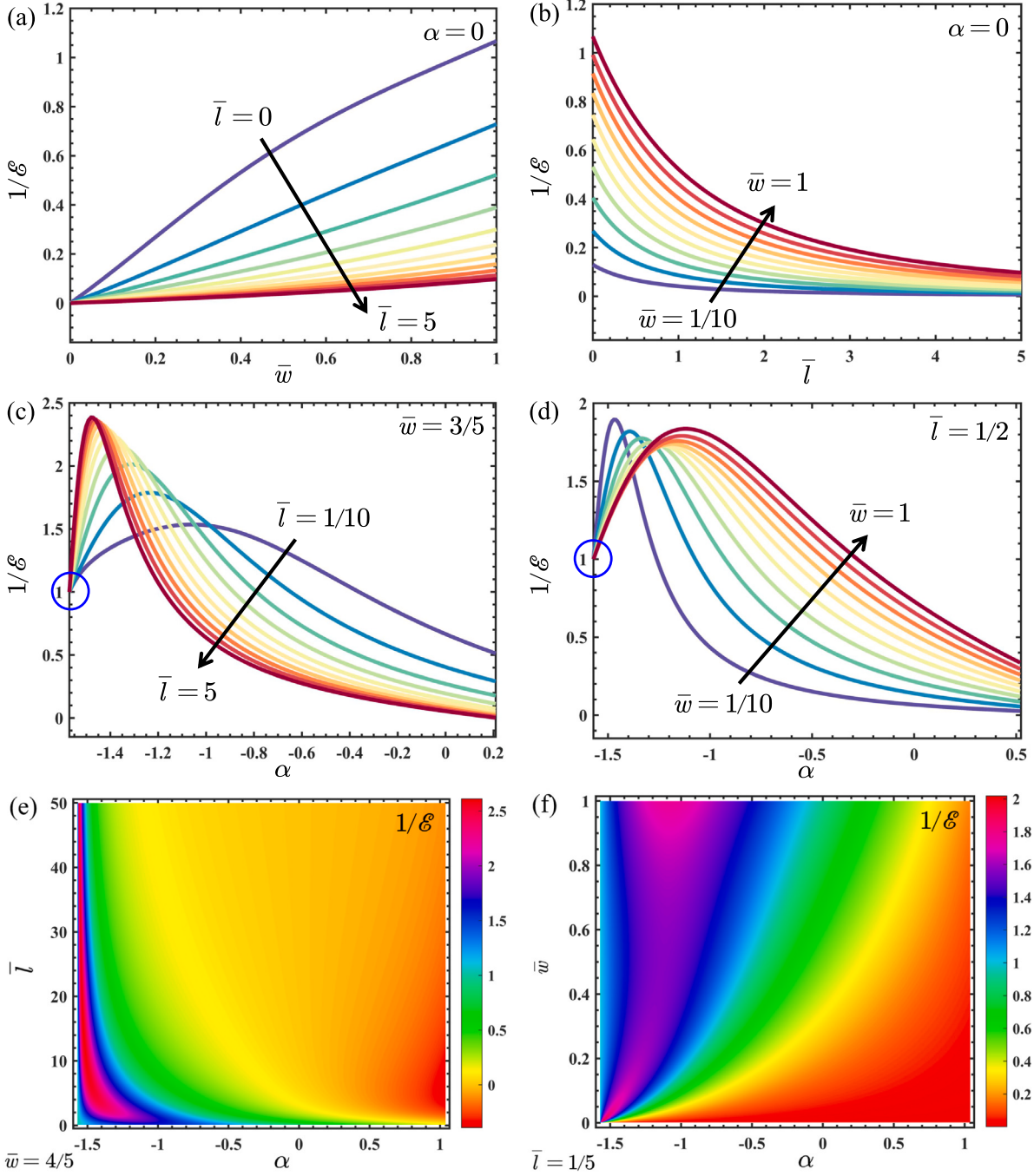


Fig. 6. Geometry dependence and distribution of the normalized stretchability \mathcal{E} for the varying \bar{w} , α and \bar{l} . (a) The reciprocal of normalized stretchability versus \bar{w} when $\alpha = 0$ and $0 \leq \bar{l} \leq 5$. (b) The reciprocal of normalized stretchability versus \bar{l} when $\alpha = 0$ and $1/10 \leq \bar{w} \leq 1$. (c) The reciprocal of normalized stretchability as the function of α when $\bar{w} = 3/5$ and $1/10 \leq \bar{l} \leq 5$. (d) The reciprocal of normalized stretchability as the function of α when $\bar{l} = 1/2$ and $1/10 \leq \bar{w} \leq 1$. (e) Distribution of the reciprocal of normalized stretchability when $\bar{w} = 4/5$. (f) Distribution of the reciprocal of normalized stretchability when $\bar{l} = 1/5$. (Online version in colour.)

the highest stretchability in serpentine-based devices. Derived from meticulous experiments and rigorous testing, our findings reveal a substantial enhancement in the flexibility and stretchability of the serpentine with large curvature. This significant improvement paves the way for their auspicious integration into flexible devices. In the realm of bioelectronics, serpentine with various degrees of curvature demonstrate an impressive capacity to adapt to the dynamic environment of biological systems without compromising their functionality.

In the context of communication technology, the augmented flexibility could be instrumental in the evolution of wearable and portable devices that necessitate high conformability. Moreover, within the domains of photovoltaics and energy storage, these findings insinuate the potential to devise more efficient, flexible solar cells and batteries that can be seamlessly integrated onto diverse surfaces. Further, these results not only broaden the design horizons for ultrastretchable serpentine ribbons with large curvature, but also pioneer a new benchmark for their performance in the face of extreme deformation.

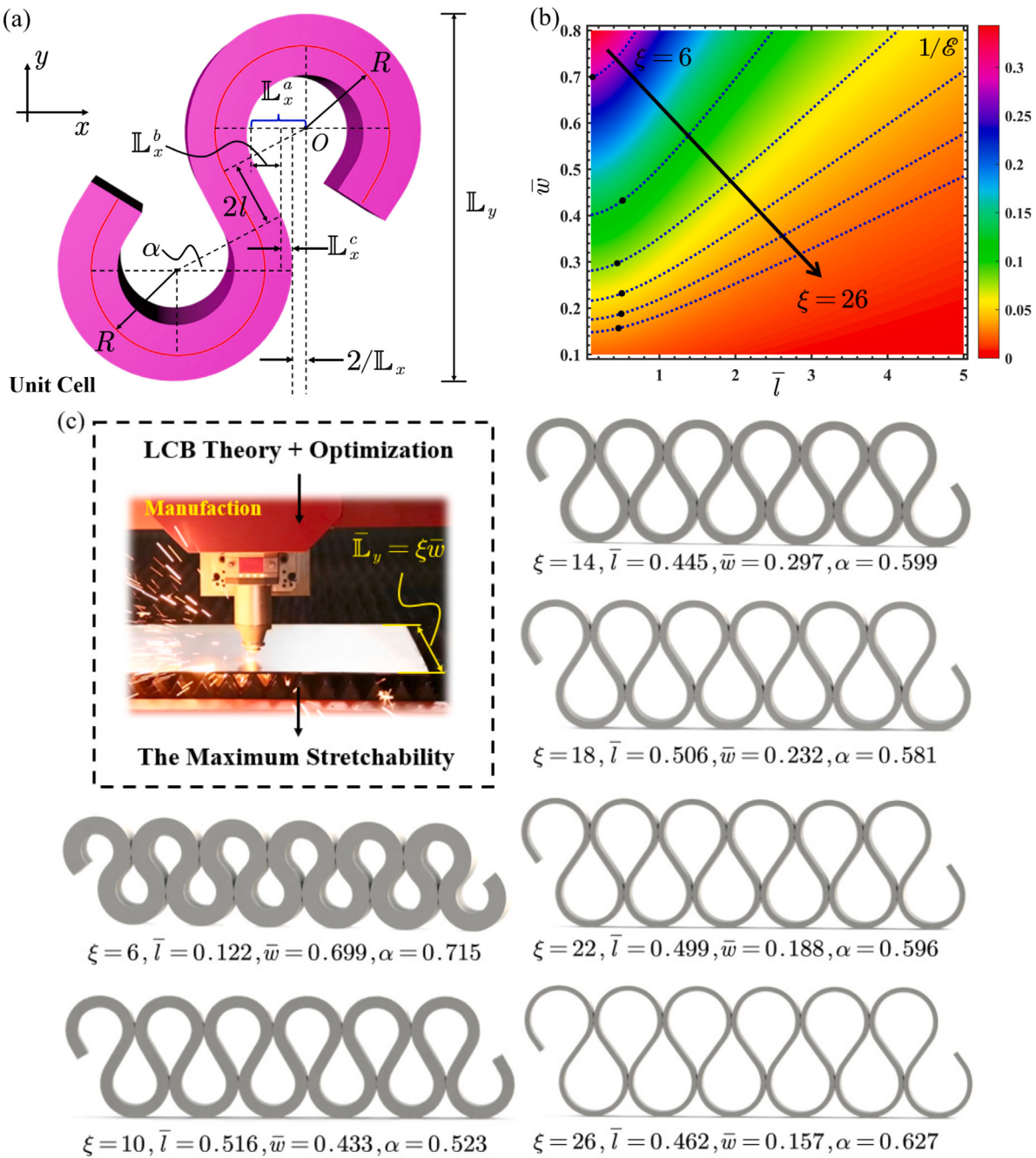


Fig. 7. Optimization analysis and design for the ultrastretchable serpentine ribbon with geometrically constrained conditions. (a) Non-overlapping geometry nature and geometrically constrained conditions in the unit cell. (b) Distribution of the reciprocal of normalized stretchability for \bar{l} and \bar{w} when the degree of geometric restriction $6 \leq \xi \leq 26$. (c) The final optimized serpentine shapes, with maximum normalized stretchability, under various geometry constraints for the range of $6 \leq \xi \leq 26$. Here, ξ represents a prefactor that indicates the degree of geometrical restriction. For different values of ξ , the corresponding optimized shapes are characterized by $\{\bar{l}, \bar{w}, \alpha\}$. (Online version in colour.)

Declaration of competing interest

The authors declare that they have no known competing financial interests or personal relationships that could have appeared to influence the work reported in this paper.

Data availability

Data will be made available on request.

Acknowledgements

This work was supported by the National Natural Science Foundation of China (Grant nos. 12202105, 12122204, 12072094, and 11872150), the China National Postdoctoral Program for Innovative Talents (Grant no. BX20220086), the China Postdoctoral Science Foundation (Grant no. 2022M710751), Shanghai Post-doctoral Excellence Program, China (Grant No. 2022732), Shanghai Pilot Program for Basic Research-Fudan University, China (Grant No. 21TQ1400100-21TQ010), and Shanghai Shuguang Program, China (Grant No. 21SG05).

Appendix A. Large curvature beam theory

We can define the normalized flexibility as

$$D = u_a F' / u'_a F = 2u_a EA / F \mathcal{L}_x \quad (\text{A.1})$$

where $\mathcal{L}_x = 4(R \cos \alpha - l \sin \alpha)$ represents the end-to-end length of the unit cell. The expression u_a/F corresponds to the flexibility of the serpentine ribbon, while u'_a/F' is the flexibility of a straight beam. The internal force equilibrium of a LCB as detailed in Fig. 2c gives

$$N_{Arc} = F \cos \theta, \quad V_{Arc} = F \sin \theta, \quad M_{Arc} = FR(1 - \cos \theta) - M_o \quad (\text{A.2})$$

$$\begin{aligned} N_{Arm} &= -F \sin \alpha, \quad V_{Arm} = F \cos \alpha, \\ M_{Arm} &= F(R + R \sin \alpha + s_2 \cos \alpha) - M_o \end{aligned} \quad (\text{A.3})$$

where N and V represent the internal axial, shear forces, respectively. M is the internal moment for the LCB.

Utilizing the energy method and boundary condition for $\theta = 0$, we can link the unknown M_o and generalized displacement using the following relation, that is

$$\partial \mathbb{U} / \partial M_o = \partial (\mathbb{U}_{Arc} + \mathbb{U}_{Arm}) / \partial M_o = 0 \quad (\text{A.4})$$

where $\mathbb{U} = \mathbb{U}_{Arc} + \mathbb{U}_{Arm}$ is the elastic strain energy.

Previous theoretical construction of curved beams with respect to serpentine ribbon is found to be only applicable to $\bar{w} = w/R < 1/5$. According to the LCB theory, we develop the extended model formulation for the serpentine ribbon with $\bar{w} \geq 1/5$ (such as $\bar{w} = 1$). For the arc section in Fig. 2, the strain energy \mathbb{U}_{Arc} can be calculated by

$$\mathbb{U}_{Arc} = \int_0^{(\pi/2+\alpha)R} \left(\frac{M_{Arc}^2}{2ESR} + \frac{M_{Arc} N_{Arc}}{EAR} + \frac{N_{Arc}^2}{2EA} + \kappa V_{Arc}^2 / 2GA \right) ds_1 \quad (\text{A.5})$$

as to the strain energy of arm section \mathbb{U}_{Arm}

$$\mathbb{U}_{Arm} = \int_0^l \left(\frac{N_{Arm}^2}{2EA} + \kappa V_{Arm}^2 / 2GA + \frac{M_{Arm}^2}{2EI} \right) ds_2 \quad (\text{A.6})$$

where G is shear modulus, κ is the energy correction coefficient, $A = w$ is the area of cross section, $I = w^3/12$ represents the second-area moment of cross section, $S = JwR$ is the static moment of the cross section on neutral axis, indicating the large curvature effects, and $J = 1 - \bar{w}/(\ln(2 + \bar{w}) - \ln(2 - \bar{w}))$. $E = E'/(1 - \mu'^2)$ and E' are plane strain modulus and Young's modulus, respectively. μ' represents the Poisson's ratio.

According to Eqs. (A.5) and (A.6), the generalized displacements with regard to arc and arm can be given by

$$\begin{aligned} \partial \mathbb{U}_{Arc} / \partial M_o &= (A(M_o - FR)(\pi + 2\alpha) + 2F(AR - S)\cos \alpha) / 2AES \\ \partial \mathbb{U}_{Arm} / \partial M_o &= l(2M_o - 2FR - Fl\cos \alpha - 2FR\sin \alpha) / 2EI \end{aligned} \quad (\text{A.7})$$

By plugging Eq. (A.7) into the boundary condition from Eq. (A.4), we obtain

$$M_o = F \left(\frac{AR(I\pi + 2IS + 2I\alpha + 2IS\sin \alpha)}{(2IS + Al^2S - 2AIR)\cos \alpha} \right) (A(2IS + I(\pi + 2\alpha)))^{-1} \quad (\text{A.8})$$

To establish the normalized flexibility of serpentine ribbon with the LCB, the relationship between the loading and displacement needs to be refined. With the M_o in hand, Moore Integral method can be adopted to calculate the displacement $u_a = 2(\delta_{Arc} + \delta_{Arm})$ corresponding to F , as to δ_{Arc} and δ_{Arm}

$$\delta_{Arc} = \int_0^{(\pi/2+\alpha)R} \left(\frac{M_{Arc} \bar{M}_{Arc}}{ESR} + \frac{N_{Arc} \bar{M}_{Arc}}{EAR} + \frac{M_{Arc} \bar{N}_{Arc}}{EAR} + \frac{N_{Arc} \bar{N}_{Arc}}{EA} + \kappa V_{Arc} \bar{V}_{Arc} / GA \right) ds_1 \quad (\text{A.9})$$

$$\delta_{Arm} = \int_0^l (M_{Arm} \bar{M}_{Arm} / EI + N_{Arm} \bar{N}_{Arm} / EA + \kappa V_{Arm} \bar{V}_{Arm} / GA) ds_2$$

where \bar{N} , \bar{V} and \bar{M} are the internal force components of the LCB when $F = 1$. By substituting Eq. (A.9) and applied displacement u_a into Eq. (A.1), the normalized flexibility can be written in terms of the dimensionless form as

$$D = (\bar{w}^4 d_1 + \mathcal{J}^2 d_2 + \mathcal{J} \bar{w}^2 d_3 + \cos(2\alpha) d_4 + \sin(2\alpha) d_5) / d_6 \quad (\text{A.10})$$

where

$$\begin{aligned} d_1 &= 25(d^* - 2)(d^* + 2) \\ d_2 &= 4(300\bar{l}^4 + 936\bar{l}^2 \bar{w}^2 - 25\bar{w}^4 + 318\bar{l}\bar{w}^2 d^*) \\ d_3 &= 1200\bar{l}^2 + 200\bar{l}^3 d^* + 2\bar{l}(600 + 103\bar{w}^2)d^* + \bar{w}^2(200 + 53(d^*)^2) \\ d_4 &= 2 \left(100\mathcal{J}\bar{w}^4 - 50\bar{w}^4 + \mathcal{J}^2(600\bar{l}^4 + 672\bar{l}^2 \bar{w}^2 - 50\bar{w}^4) \right. \\ &\quad \left. + \mathcal{J}\bar{w}^2(600\bar{l} + 100\bar{l}^2 d^* + (53\bar{w}^2 - 300)d^*) \right) \\ d_5 &= \bar{w}^2(\mathcal{J}(1800\bar{l} + 600\bar{l}^2 d^* + 103\bar{w}^2 d^*) + 72\mathcal{J}^2\bar{l} - 25\bar{w}^2 d^*) \\ d_6 &= 100\mathcal{J}\bar{w}^2(24\mathcal{J}\bar{l} + (2\alpha + \pi)\bar{w}^2)(\cos \alpha - \bar{l}\sin \alpha) \\ d^* &= \pi + 2\alpha \end{aligned} \quad (\text{A.11})$$

The second key mechanic index is normalized stretchability, it can be given using the following relation:

$$\mathcal{E} = \varepsilon_a^f / \varepsilon_m^f = \varepsilon_a / \varepsilon_{\max} \quad (\text{A.12})$$

The applied strain can be determined as $\varepsilon_a = 2u_a/\mathcal{L}_x$, and aim of the next step is to calculate the maximum strain of the LCB. According to the LCB theory, the hoop stress can be written as

$$\sigma_{Arc} = M_{Arc}y/S(R - Sw^{-1} + y) + N_{Arc}/A \quad (\text{A.13})$$

Applying the physical equation, the peak strain ε_{\max} at the inner arc crest can be calculated by

$$\varepsilon_{\max} = E^{-1}(-M_o(2S - w^2)/S(2Rw - w^2) + F/A) \quad (\text{A.14})$$

Finally, by substituting ε_a and Eq. (A.14) into Eq. (A.12), we have

$$\mathcal{E} = (\bar{w}^4 d_1 + \mathcal{J}^2 d_2 + \mathcal{J} \bar{w}^2 d_3 + \cos(2\alpha) d_4 + \sin(2\alpha) d_5) / d_7 \quad (\text{A.15})$$

where $d_1 \sim d_5$ are provided in Eq. (A.11), d_7 and d_8 are given as follows:

$$\begin{aligned} d_7 &= 100\bar{w}^2(\cos \alpha - \bar{l}\sin \alpha)d_8/(\bar{w} - 2) \\ d_8 &= \left(\frac{2(2\mathcal{J} - \bar{w})((6\mathcal{J}\bar{l}^2 + (\mathcal{J} - 1)\bar{w}^2)\cos \alpha + 12\mathcal{J}\bar{l}\sin \alpha)}{+(\mathcal{J} - 1)\bar{w}(24\mathcal{J}\bar{l} + \bar{w}^2(\pi + 2\alpha))} \right) \end{aligned} \quad (\text{A.16})$$

Appendix B. Elasticity theory

For the specific geometry (i.e., $\alpha = \bar{l} = 0$), curvilinear coordinates (r, θ) and elasticity theory can be used to obtain the exact solution for the serpentine ribbon. Based on the Airy stress function, function Φ must satisfy the following partial differential equation (PDE), i.e.,

$$(\partial^2 / \partial r^2 + r^{-1} \partial / \partial r + r^{-2} \partial^2 / \partial \theta^2)(\partial^2 \Phi / \partial r^2 + r^{-1} \partial \Phi / \partial r + r^{-2} \partial^2 \Phi / \partial \theta^2) = 0 \quad (\text{B.1})$$

Then, let $\Phi = \varphi(r) \sin \theta$, Eq. (B.1) (PDE) reduces to the following ordinary differential equation (ODE)

$$(d^2 / dr^2 + r^{-1} d / dr - r^{-2})(d^2 \varphi / dr^2 + r^{-1} d \varphi / dr - \varphi r^{-2}) = 0 \quad (\text{B.2})$$

based on which we can identify the general solution with respect to $\varphi(r)$, that is

$$\varphi(r) = Ar^3 + Br^{-1} + Cr + Dr \ln r \quad (\text{B.3})$$

where A , B , C and D are undetermined constants. Therefore, the Airy stress function can be given by

$$\Phi(r, \theta) = (Ar^3 + Br^{-1} + Cr + Dr \ln r) \sin \theta \quad (\text{B.4})$$

In the polar coordinates, the stress field can be calculated by

$$\begin{aligned}\sigma_r &= r^{-1} \partial \Phi / \partial r + r^{-2} \partial^2 \Phi / \partial \theta^2 \\ \sigma_\theta &= \partial^2 \Phi / \partial r^2 \\ \tau_{r\theta} &= -(\partial / \partial r) r^{-1} \partial \Phi / \partial \theta\end{aligned}\quad (\text{B.5})$$

Combination of Eqs. (B.4) and (B.5) gives the following expressions for achieving the stress components

$$\begin{aligned}\sigma_r &= (2Ar - 2Br^{-3} + Dr^{-1}) \sin \theta \\ \sigma_\theta &= (6Ar + 2Br^{-3} + Dr^{-1}) \sin \theta \\ \tau_{r\theta} &= -(2Ar - 2Br^{-3} + Dr^{-1}) \cos \theta\end{aligned}\quad (\text{B.6})$$

According to the boundary conditions $\sigma_r|_{r=a,b} = \tau_{r\theta}|_{r=a,b} = 0$, we have

$$2Aa - 2Ba^{-3} + Da^{-1} = 0 \quad \text{and} \quad 2Ab - 2Bb^{-3} + Db^{-1} = 0 \quad (\text{B.7})$$

Moreover, the external force F can be expressed using the following relationship

$$F = \int_a^b \tau_{r\theta} dr = A(b^2 - a^2) - B(b^2 - a^2)a^{-2}b^{-2} + D \ln(b/a) \quad (\text{B.8})$$

Based on Eqs. (B.7) and (B.8), the undetermined constants can be given by

$$\begin{aligned}A &= -F/2\mathcal{N}, \quad B = Fa^2b^2/2\mathcal{N}, \quad D = F(a^2 + b^2)/\mathcal{N} \\ \mathcal{N} &= (a^2 - b^2) + (a^2 + b^2) \ln(b/a), \quad a = R - w/2, \quad b = R + w/2\end{aligned}\quad (\text{B.9})$$

Assuming that the maximum stress point is fixed, from Eqs. (B.6) and (B.9) we obtain the peak strain

$$\varepsilon_{\max} = F((a^2 + b^2)a^{-1} + a^{-1}b^2 - 3a)/E\mathcal{N} \quad (\text{B.10})$$

Next, we consider the displacement field induced by the external applied loading. Based on the expressions of strain components in polar coordinates, we have

$$du/\partial r = (\sin \theta/E)(2Ar(1 - 3\mu) - 2Br^{-3}(1 + \mu) + Dr^{-1}(1 - \mu)) \quad (\text{B.11})$$

$$dv/\partial \theta = r\epsilon_\theta - u \quad (\text{B.12})$$

$$\gamma_{r\theta} = r^{-1} \partial u / \partial \theta + \partial v / \partial r - v/r \quad (\text{B.13})$$

First, we perform the indefinite integral with regard to Eq. (B.11), where \mathbb{F}_1 is the function of θ only, this yields

$$u = (E^{-1} \sin \theta)(\mathcal{A}r^2(1 - 3\mu) + Br^{-2}(1 + \mu) + D(1 - \mu) \ln r) + \mathbb{F}_1 \quad (\text{B.14})$$

Second, by substituting $\epsilon_\theta = E^{-1}(\sigma_\theta - \mu\sigma_r)$ and Eq. (B.14) into Eq. (B.12), we obtain the displacement v , that is

$$v = (E^{-1} \cos \theta) \left(\begin{array}{l} -\mathcal{A}r^2(5 + \mu) - Br^{-2}(1 + \mu) \\ + D(1 - \mu) \ln r - D(1 - \mu) \end{array} \right) - \int \mathbb{F}_1 d\theta + \mathbb{F}_2 \quad (\text{B.15})$$

where \mathbb{F}_2 is the function of r only, and $\mu = \mu'/(1 - \mu')$.

Next, according to Eqs. (B.13), (B.14) and (B.15), the unknown functions regarding $\mathbb{F}_1(\theta)$ and $\mathbb{F}_2(r)$ satisfy the following equation

$$\int \mathbb{F}_1(\theta) d\theta + \mathbb{F}'_1(\theta) + r\mathbb{F}'_2(r) - \mathbb{F}_2(r) = \mathbb{F}^* \quad (\text{B.16})$$

where $\mathbb{F}^* = -4E^{-1}D \cos \theta$.

Then, we let $\mathbb{F}_1(\theta) = \mathcal{K} \sin \theta + \mathcal{L} \cos \theta + \mathbb{F}^* \theta/2$ and $\mathbb{F}_2(r) = \mathcal{H}r$, where \mathcal{K} , \mathcal{L} and \mathcal{H} are the arbitrary constants, the strain components can be expressed as follows

$$\begin{aligned}u &= \left(\begin{array}{l} -2E^{-1}D\theta \cos \theta + \mathcal{K} \sin \theta + \mathcal{L} \cos \theta \\ + (E^{-1} \sin \theta)(\mathcal{A}r^2(1 - 3\mu) + Br^{-2}(1 + \mu) + D(1 - \mu) \ln r) \end{array} \right) \\ v &= \left(\begin{array}{l} 2E^{-1}D\theta \sin \theta + (E^{-1} \cos \theta) \left(\begin{array}{l} -\mathcal{A}r^2(5 + \mu) - Br^{-2}(1 + \mu) \\ + D(1 - \mu) \ln r - D(1 - \mu) \end{array} \right) \\ + E^{-1}D(1 + \mu) \cos \theta + \mathcal{K} \cos \theta - \mathcal{L} \sin \theta + \mathcal{H}r \end{array} \right)\end{aligned}\quad (\text{B.17})$$

Using the boundary conditions, i.e. $v|_{\theta=\pi/2} = \partial v / \partial r|_{\theta=\pi/2} = 0$, we can obtain $\mathcal{H} = 0$ and $\mathcal{L} = E^{-1}D\pi$, based on which the applied displacement u_a and applied strain ϵ_a corresponding to the external force F can be calculated as

$$u_a = 2E^{-1}D\pi \quad \text{and} \quad \epsilon_a = R^{-1}E^{-1}D\pi \quad (\text{B.18})$$

Finally, by plugging Eqs. (B.18) and (B.10) into Eq. (B.12), the following expression can be used to solve the normalized stretchability \mathcal{E} with respect to elasticity theory, that is

$$\mathcal{E} = a(b^2 + a^2)\pi/(b - a)(b + a)^2 = \pi(2 - \bar{w})(4 + \bar{w}^2)/16\bar{w} \quad (\text{B.19})$$

where $a = R - w/2$ and $b = R + w/2$ represent the inner and outer radii for the arbitrary curved beam, respectively.

Appendix C. Conventional beam theory

On the one hand, by taking the expansion of $\ln(b/a)$ from the elasticity theory, we have

$$\ln(b/a) = \ln(1 + w/a) = w/a - w^2/2a^2 + w^3/3a^3 + \mathcal{O}(w^3) \quad (\text{C.1})$$

The applied displacement (see Eq. (B.18) in Appendix B for details) to the three orders reads

$$u_a = 6a^3 F \pi / E w^3 \quad (\text{C.2})$$

which is the well-known deflection solution in the preliminary material mechanics.

On the other hand, the LCB theory gives the following relationship for achieving the pure bending stress σ

$$\sigma = My \left((1 + y/R(1 - \mathcal{J})) \int_A \frac{y^2}{1 + y/R(1 - \mathcal{J})} dA \right)^{-1} \quad (\text{C.3})$$

If we neglect the curvature effects, i.e., $y/R(1 - \mathcal{J}) \ll 1$, Eq. (C.3) reduces to

$$\sigma = My / \int_A y^2 dA = My/I \quad (\text{C.4})$$

which is the well-known bending stress formula, and I represents the so-called second-area moment of cross section in the CB theory.

For the sake of simplicity, the similar procedure (see Appendix A for details) can be used to identify the normalized flexibility and stretchability. Due to the limitations of the conventional beam theory, the final expressions cannot be applicable to the serpentine ribbons with LCB in flexible devices.

The internal forces and moments are provided in Eqs. (A.2) and (A.3). According to the energy principle, strain energy expressions regarding the arc and arm sections can be written by

$$\begin{aligned}\mathbb{U}_{\text{Arc}} &= \int_0^{(\pi/2+\alpha)R} (N_{\text{Arc}}^2/2EA + \kappa V_{\text{Arc}}^2/2GA + M_{\text{Arc}}^2/2EI) ds_1 \\ \mathbb{U}_{\text{Arm}} &= \int_0^l (N_{\text{Arm}}^2/2EA + \kappa V_{\text{Arm}}^2/2GA + M_{\text{Arm}}^2/2EI) ds_2\end{aligned}\quad (\text{C.5})$$

The boundary condition $(\partial \mathbb{U} / \partial M_o)|_{\theta=0} = 0$ yields the following equation for identifying the unknown M_o , we have

$$M_o = F(R(2l + \pi R + 2R\alpha + 2l \sin \alpha) + (l^2 - 2R^2) \cos \alpha)/(2l + R(\pi + 2\alpha)) \quad (\text{C.6})$$

Correspondingly, the displacements with regard to δ_{Arc} and δ_{Arm} can be calculated using

$$\begin{aligned}\delta_{\text{Arc}} &= \int_0^{(\pi/2+\alpha)R} (M_{\text{Arc}} \bar{M}_{\text{Arc}}/EI + N_{\text{Arc}} \bar{N}_{\text{Arc}}/EA + \kappa V_{\text{Arc}} \bar{V}_{\text{Arc}}/GA) ds_1 \\ \delta_{\text{Arm}} &= \int_0^l (M_{\text{Arm}} \bar{M}_{\text{Arm}}/EI + N_{\text{Arm}} \bar{N}_{\text{Arm}}/EA + \kappa V_{\text{Arm}} \bar{V}_{\text{Arm}}/GA) ds_2\end{aligned}\quad (\text{C.7})$$

Combining Eqs. (A.1) and (C.7), the normalized flexibility from the CB theory can be given by

$$D = (\tilde{d}_1 + \cos(2\alpha)\tilde{d}_2 + \sin(2\alpha)\tilde{d}_3)/\tilde{d}_4 \quad (C.8)$$

where

$$\begin{aligned} \tilde{d}_1 &= \left(100\bar{l}^4 - 1200 + 4\bar{l}^2(300 + 103\bar{w}^2) + 200\bar{l}^3 d^* \right. \\ &\quad \left. + 4\bar{l}(300 + 103\bar{w}^2)d^* + (300 + 103\bar{w}^2)(d^*)^2 \right) \\ \tilde{d}_2 &= 2(50\bar{l}^4 - 600 + 2\bar{l}^2(53\bar{w}^2 + 300) + 100\bar{l}^3 d^* + \bar{l}(53\bar{w}^2 - 300)d^*) \\ \tilde{d}_3 &= 2\bar{l}(900 + 53\bar{w}^2) + 600\bar{l}^2 d^* + (53\bar{w}^2 - 300)d^* \\ \tilde{d}_4 &= 100\bar{w}^2(2\bar{l} + d^*) (\cos \alpha - \bar{l} \sin \alpha) \end{aligned} \quad (C.9)$$

Next, the second key index, i.e., the normalized stretchability of serpentine ribbons, will be demonstrated based on Eq. (A.12). Applying the stress expression in Eq. (C.4) and physical equation, the maximum strain can be given by

$$\varepsilon_{\max} = (-M_o y/EI) \Big|_{\theta=0, y=-w/2} \quad (C.10)$$

Finally, based on the applied strain ε_a and ε_{\max} , the normalized stretchability \mathcal{E} in terms of three dimensionless parameters can be given as

$$\mathcal{E} = (\tilde{d}_1 + \cos(2\alpha)\tilde{d}_2 + \sin(2\alpha)\tilde{d}_3)/\tilde{d}_5 \quad (C.11)$$

where

$$\tilde{d}_5 = 600\bar{w}(\cos \alpha - \bar{l} \sin \alpha)(2\bar{l} + d^* + (\bar{l}^2 - 2) \cos \alpha + 2\bar{l} \sin \alpha) \quad (C.12)$$

Appendix D. Important approximate solutions

To guide the multifunctional design of the ultrastretchable serpentine ribbon in flexible devices, we provide some useful analytical results with respect to the normalized flexibility and normalized stretchability:

Case I: The serpentine ribbon without the arc angle.

$$\left\{ \begin{array}{l} D \approx 103\pi/100 + 78\bar{l}/25 + \hat{d}_1/(2\bar{l} + \pi) \bar{w}^2 \\ \hat{d}_1 = 24\bar{l}^2 + 2\bar{l}^4 + 6\bar{l}\pi + 4\bar{l}^3\pi + 3(\pi^2 - 8) \end{array} \right. \quad (D.1)$$

$$\left\{ \begin{array}{l} \mathcal{E} \approx (100\hat{d}_2 + (2\bar{l} + \pi)(312\bar{l} + 103\pi)\bar{w}^2)/\hat{d}_3 \\ \hat{d}_2 = 24\bar{l}^2 + 2\bar{l}^4 + 6\bar{l}\pi + 4\bar{l}^3\pi + 3(\pi^2 - 8) \end{array} \right. \quad (D.2)$$

$$\left\{ \begin{array}{l} \hat{d}_3 = 600(\bar{l}(2 + \bar{l}) + \pi - 2)\bar{w} \end{array} \right. \quad (D.2)$$

Case II: The serpentine ribbon without the arm section.

$$\left\{ \begin{array}{l} D \approx (\hat{d}_4 \sec \alpha + \hat{d}_5)/100\bar{w}^2 \\ \hat{d}_4 = (300 + 103\bar{w}^2)(\pi + 2\alpha) \end{array} \right. \quad (D.3)$$

$$\left\{ \begin{array}{l} \hat{d}_5 = 2(53\bar{w}^2 - 300)\sin \alpha - 2400(\pi + 2\alpha)^{-1} \cos \alpha \end{array} \right. \quad (D.4)$$

$$\left\{ \begin{array}{l} \mathcal{E} \approx ((\pi + 2\alpha)\hat{d}_6 - 2400 \cos \alpha)/\hat{d}_7 \\ \hat{d}_6 = (300 + 103\bar{w}^2)(\pi + 2\alpha) \sec \alpha + 2(53\bar{w}^2 - 300)\sin \alpha \end{array} \right. \quad (D.4)$$

$$\left\{ \begin{array}{l} \hat{d}_7 = 600\bar{w}(\pi + 2\alpha - 2 \cos \alpha) \end{array} \right. \quad (D.4)$$

Case III: The serpentine ribbon without the arc angle and arm section.

$$D \approx 103\pi/100 + 3(\pi^2 - 8)/\pi\bar{w}^2 \quad (D.5)$$

$$\mathcal{E} \approx (\pi^2(300 + 103\bar{w}^2) - 2400)/600(\pi - 2)\bar{w} \quad (D.6)$$

Appendix E. Experimental data

See Fig. E.1.

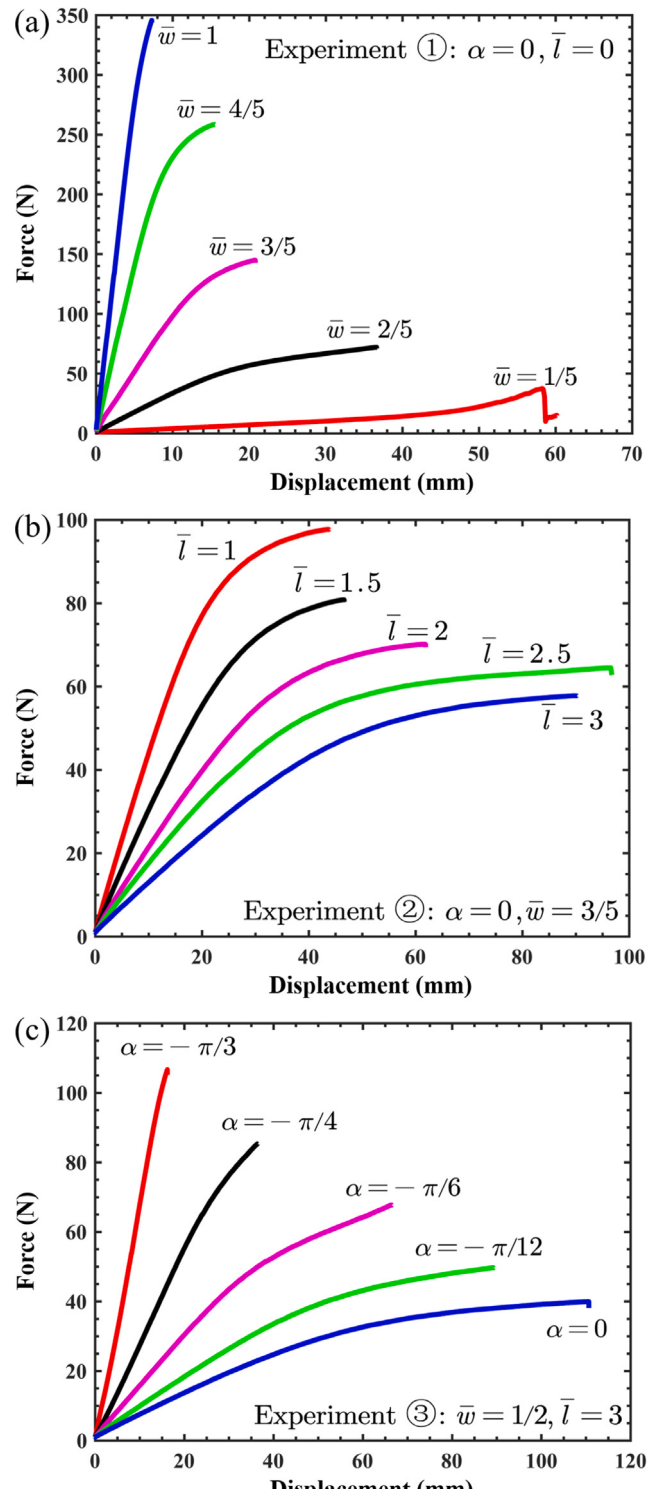


Fig. E.1. Force–displacement curves for various serpentine ribbons corresponding to Fig. 3a.

References

- Ashley, B.K., Brown, M.S., Park, Y., Kuan, S.-Y., Koh, A., 2019. Skin-inspired, open mesh electrochemical sensors for lactate and oxygen monitoring. *Biosens. Bioelectron.* 132, 343–351.
- Brosteaux, D., Aghassi-Hagmann, J., Gonzalez, M., Vanfleteren, J., 2007. Design and fabrication of elastic interconnections for stretchable electronic circuits. *IEEE Electr. Dev. Lett.* 28, 552–554.

- Chung, H.U., Rwei, A.Y., Hourlier-Fargette, A., Xu, S., Lee, K., Dunne, E.C., Xie, Z., Liu, C., Carlini, A., Kim, D.H., et al., 2020. Skin-interfaced biosensors for advanced wireless physiological monitoring in neonatal and pediatric intensive-care units. *Nature Med.* 26 (3), 418–429.
- Cicconofri, G., DeSimone, A., 2015. A study of snake-like locomotion through the analysis of a flexible robot model. *Proc. R. Soc. Lond. Ser. A Math. Phys. Eng. Sci.* 471 (2182), 20150054.
- Coulais, C., Teomy, E., de Reus, K., Shokef, Y., van Hecke, M., 2016. Combinatorial design of textured mechanical metamaterials. *Nature* 535 (7611), 529–532.
- Fan, J.A., Yeo, W.-H., Su, Y., Hattori, Y., Lee, W.-K., Jung, S.-Y., Zhang, Y., Liu, Z., Cheng, H., Falgout, L., Bajema, M., Coleman, T., Gregoire, D., Larsen, R.J., Huang, Y., Rogers, J.A., 2014. Fractal design concepts for stretchable electronics. *Nature Commun.* 5, 3266.
- Fan, Z., Zhang, Y., Ma, Q., Zhang, F., Fu, H., Hwang, K., Huang, Y., 2016. A finite deformation model of planar serpentine interconnects for stretchable electronics. *Int. J. Solids Struct.* 91, 46–54.
- Frenzel, T., Findeisen, C., Kadlec, M., Gumbsch, P., Wegener, M., 2016. Tailored buckling microlattices as reusable lightweight shock absorbers. *Adv. Mater.* 28 (30), 5865–5870.
- Fu, H., Nan, K., Bai, W., Huang, W., Bai, K., Lu, L., Zhou, G., Han, M., Yan, Z., Luan, H., Wang, Q., Guo, R., Zhang, Y., Luo, Y., Huang, Y., Rogers, J.A., 2018. Morphable 3D mesostructures and microelectronic devices by multistable buckling mechanics. *Nature Mater.* 17, 268–276.
- Guan, Y., Li, H., Ren, F., Ren, S., 2018a. Kirigami-inspired conducting polymer thermoelectrics from electrostatic recognition driven assembly. *ACS Nano* 12 (8), 7967–7973.
- Guan, Y., Zhang, Z., Tang, Y., Yin, J., Ren, S., 2018b. Kirigami-inspired nanoconfined polymer conducting nanosheets with 2000 percent stretchability. *Adv. Mater.* 30 (8), e1706390.
- Hong, Y.J., Jeong, H.Y., Cho, K.-W., Lu, N., Kim, D.-H., 2019. Wearable and implantable devices for cardiovascular healthcare: from monitoring to therapy based on flexible and stretchable electronics. *Adv. Funct. Mater.* 29.
- Hong, S., Lee, H., Lee, J.-H., Kwon, J., Han, S., Suh, Y., Cho, H., Shin, J., Yeo, J.C., Ko, S.H., 2015. Highly stretchable and transparent metal nanowire heater for wearable electronics applications. *Adv. Mater.* 27, 4744–4751.
- Hwang, D., Barron, Jr., E., Haque, A., Bartlett, M., 2022. Shape morphing mechanical metamaterials through reversible plasticity. *Science Robotics* 7, eabg2171.
- Jang, K., Li, K., Chung, H., Xu, S., Jung, H., Yang, Y., Jung, H., Song, J., Yang, J., Kim, J., Lee, J., Kim, G., Cho, K., Park, J., Kim, J., Lee, C., Kim, S., Lee, Y., Kim, J., Choi, J., Lee, T., Hyeon, T., Kim, D., Choi, S., Kim, T., Huang, Y., Rogers, J., 2017. Self-assembled three dimensional network designs for soft electronics. *Nature Commun.* 8, 15894.
- Jang, K.-I., Li, K., Chung, H.-J., Xu, S., Jung, H.-T., Yang, Y., Kwak, J.H., Jung, H.J., Song, J.-H., Yang, H.-J., et al., 2015. Soft network composite materials with deterministic and bio-inspired designs. *Nature Commun.* 6, 6566.
- Jeong, G.-S., Baek, D.-H., Jung, H.-Y.C., Song, J., Moon, J.-H., Hong, S.-C., Kim, I., Lee, S.-H., 2012. Solderable and electroplatable flexible electronic circuit on a porous stretchable elastomer. *Nature Commun.* 3, 977.
- Jeong, J.-W., Yeo, W.-H., Akhtar, A., Norton, J.J.S., Kwack, K.-S., Li, S., Jung, S.-Y., Su, Y., Lee, W.-K., Xia, J., Cheng, H., Huang, Y., Choi, W.-H., Bretl, T., Rogers, J.A., 2013. Materials and optimized designs for human-machine interfaces via epidermal electronics. *Adv. Mater.* 25, 6839–6846.
- Jin, L., Forte, A., Bertoldi, K., 2021. Mechanical valves for on-board flow control of inflatable robots. *Adv. Sci. (Weinh.)* 8 (18), 2101941.
- Kim, Y., van den Berg, J., Crosby, A., 2021. Autonomous snapping and jumping polymer gels. *Nature Mater.*
- Kim, D.-H., Lu, N., Ma, R., Kim, Y.-S., Kim, R.-H., Wang, S., Wu, J., Won, S.M., Tao, H., Islam, A., Yu, K., Kim, T.-i., Chowdhury, R., Ying, M., Xu, L., Li, M., Chung, H.-J., Keum, H.-J., McCormick, M., Liu, P., Zhang, Y.-w., Omenetto, F.G., Huang, Y., Coleman, T., Rogers, J.A., 2011. Epidermal electronics. *Science* 333 (6044), 838–843.
- Kim, D.-H., Song, J., Choi, W.M., Kim, H.-S., Kim, R.-H., Liu, Z., Huang, Y.Y., Hwang, K.-C., Zhang, Y.-w., Rogers, J.A., 2008. Materials and noncoplanar mesh designs for integrated circuits with linear elastic responses to extreme mechanical deformations. *Proc. Natl. Acad. Sci. USA* 105, 18675–18680.
- Kim, Y., Yuk, H., Zhao, R., Chester, S., Zhao, X., 2018. Printing ferromagnetic domains for untethered fast-transforming soft materials. *Nature* 558, 274–279.
- Ko, H.C., Stoykovich, M.P., Song, J., Malyarchuk, V., Choi, W.M., Yu, C.J., Geddes, J.B., Xiao, J.L., Wang, S., Huang, Y.G., Rogers, J.A., 2008. A hemispherical electronic eye camera based on compressible silicon optoelectronics. *Nature* 454, 748–753.
- Li, S., Vogt, D.M., Rus, D., Wood, R.J., 2017. Fluid-driven origami-inspired artificial muscles. *Proc. Natl. Acad. Sci. USA* 114 (49), 13132–13137.
- Liu, Y., Boyce, M., Ortiz, C., 2016a. Guided formation of 3D helical mesostructures by mechanical buckling: Analytical modeling and experimental validation. *Adv. Funct. Mater.* 26 (18), 2909–2918.
- Liu, J., Gu, T., Shan, S., Kang, S.H., Weaver, J.C., Bertoldi, K., 2016b. Harnessing buckling to design architected materials that exhibit effective negative swelling. *Adv. Mater.* 28 (33), 6619–6624.
- Ma, Y., Zhang, Y., Kim, Y.S., Rogers, J.A., Huang, Y., 2016. Design of strain-limiting substrate materials for stretchable and flexible electronics. *Adv. Funct. Mater.* 26 (30), 5345–5351.
- Morikawa, Y., Yamagiwa, S., Sawahata, H., Numano, R., Koida, K., Ishida, M., Kawano, T., 2018. Ultrastretchable kirigami bioprosbes. *Adv. Healthc. Mater.* 7.
- Morikawa, Y., Yamagiwa, S., Sawahata, H., Numano, R., Koida, K., Kawano, T., 2019. Donut-shaped stretchable kirigami: Enabling electronics to integrate with the deformable muscle. *Adv. Healthc. Mater.* 8, e1900939.
- Pan, T., Pharr, M., Ma, Y., Ning, R., Yan, Z., Xu, R., Feng, X., Huang, Y., Rogers, J., 2017. Experimental and theoretical studies of serpentine interconnects on ultrathin elastomers for stretchable electronics. *Adv. Funct. Mater.* 27.
- Rafsanjani, A., Akbarzadeh, A., Pasini, D., 2015. Snapping mechanical metamaterials under tension. *Adv. Mater.* 27 (39), 5931–5935.
- Raney, J.R., Nadkarni, N., Daraio, C., Kochmann, D.M., Lewis, J.A., Bertoldi, K., 2016. Stable propagation of mechanical signals in soft media using stored elastic energy. *Proc. Natl. Acad. Sci. USA* 113 (35), 9722–9727.
- Shan, S., Kang, S.H., Raney, J.R., Wang, P., Fang, N., Candido, F., Lewis, J.A., Bertoldi, K., 2015. Multistable architected materials for trapping elastic strain energy. *Adv. Mater.* 27 (28), 4296–4301.
- Sim, K., Ershad, F., Zhang, Y., Yang, P., Shim, H., Rao, Z., Lu, Y., Thukral, A., Elgalad, A., Xi, Y., Tian, B., Taylor, D.A., Yu, C., 2020. An epicardial bioelectronic patch made from soft rubbery materials and capable of spatiotemporal mapping of electrophysiological activity. *Nat. Electron.* 3, 775–784.
- Someya, T., Sekitani, T., Iba, S., Kato, Y., Kawaguchi, H., Sakurai, T., 2004. A large-area, flexible pressure sensor matrix with organic field-effect transistors for artificial skin applications. *Proc. Natl. Acad. Sci. USA* 101, 9966–9970.
- Song, E., Li, J., Won, S.M., Bai, W., Rogers, J.A., 2020. Materials for flexible bioelectronic systems as chronic neural interfaces. *Nature Mater.* 19, 590–603.
- Song, Y., Min, J., Gao, W., 2019. Wearable and implantable electronics: Moving toward precision therapy. *ACS Nano* 13, 12280–12286.
- Song, L., Myers, A.C., Adams, J.J., Zhu, Y., 2014. Stretchable and reversibly deformable radio frequency antennas based on silver nanowires. *ACS Appl. Mater. Interfaces* 6 (6), 4248–4253.
- Timoshenko, G.S., 1951. Theory of Elasticity. McGraw-Hill.
- Wang, W., Li, C., Rodrigue, H., Yuan, F., Han, M.-W., Cho, M.-W., Ahn, S.H., 2017. Kirigami/origami-based soft deployable reflector for optical beam steering. *Adv. Funct. Mater.* 27 (14), 1604214.
- Wang, Y., Wang, C., 2020. Effect of temperature difference on the mechanical responses of ribbon kirigami: Toward the highly stretchable conductors. *Int. J. Mech. Sci.* 168.
- Wang, Y., Wang, C., 2021. Buckling of ultrastretchable kirigami metastructures for mechanical programmability and energy harvesting. *Int. J. Solids Struct.*.
- Wang, Y., Wang, C., 2022. Mechanics of strain-limiting wrinkled kirigami for flexible devices: High flexibility, stretchability and compressibility. *Int. J. Solids Struct.* 238.
- Wang, Y., Wang, C., Tan, H., 2020. Geometry-dependent stretchability and stiffness of ribbon kirigami based on large curvature curved beam model. *Int. J. Solids Struct.* 182–183, 236–253.
- Widlund, T., Yang, S., Hsu, Y., Lu, N., 2014. Stretchability and compliance of freestanding serpentine-shaped ribbons. *Int. J. Solids Struct.* 51, 4026–4037.
- Wu, H., Gao, W., Yin, Z., 2017. Materials, devices and systems of soft bioelectronics for precision therapy. *Adv. Healthc. Mater.* 6.
- Xu, S., Yan, Z., Jang, K.-I., Huang, W., Fu, H., Kim, J., Wei, Z., Flavin, M., McCracken, J., Wang, R., et al., 2015. Assembly of micro/nanomaterials into complex, three-dimensional architectures by compressive buckling. *Science* 347, 154–159.
- Xu, S., Zhang, Y., Jia, L., Mathewson, K.E., Jang, K.-I., Kim, H.-S., Fu, H., Huang, X., Chava, P., Wang, R., Bhole, S., Wang, L., Na, Y., Guan, Y., Flavin, M., Han, Z., Huang, Y., Rogers, J.A., 2013. Stretchable batteries with self-similar serpentine interconnects and integrated wireless recharging systems. *Nature Commun.* 4, 1543.
- Yang, S., Qiao, S., Lu, N., 2017. Elasticity solutions to nonbuckling serpentine ribbons. *J. Appl. Mech.* 84, 021004.
- Yang, C., Zhang, H., Liu, Y., Yu, Z., Wei, X., Hu, Y., 2018. Kirigami-inspired deformable 3D structures conformable to curved biological surface. *Adv. Sci. (Weinh.)* 5 (12), 1801070.
- Yeo, W.H., Kim, Y.S., Lee, J., Ameen, A., Shi, L., Li, M., Wang, S., Ma, R., Jin, S.H., Kang, Z., Huang, Y.G., Rogers, J.A., 2013. Multifunctional epidermal electronics printed directly onto the skin. *Adv. Mater.* 25, 2773–2778.
- Yin, Y., Li, M., Yuan, W., Chen, X., Li, Y., 2019. A widely adaptable analytical method for thermal analysis of flexible electronics with complex heat source structures. *Proc. R. Soc. Lond. Ser. A Math. Phys. Eng. Sci.* 475 (2222), 20190402.
- Zhang, Y., Huang, R., Rogers, J.A., 2014. Experimental and theoretical studies of serpentine microstructures bonded to prestrained elastomers for stretchable electronics. *Adv. Funct. Mater.* 24, 2028–2037.
- Zhang, F., Li, S., Shen, Z., Cheng, X., Xue, Z., Zhang, H., Song, H., Bai, K., Yan, D., Wang, H., et al., 2021. Rapidly deployable and morphable 3D mesostructures with applications in multimodal biomedical devices. *Proc. Natl. Acad. Sci. USA* 118 (11), e2026414118.
- Zhu, J., Fox, J.J., Yi, N., Cheng, H., 2019. Structural design for stretchable microstrip antennas. *ACS Appl. Mater. Interfaces* 11 (9), 8867–8877.